SCIENCE CHINA
Physics, Mechanics & Astronomy

• Article •

July 2016 Vol. 59 No. 7: 670311
doi: 10.1007/s11433-016-0056-6

Resolution of ghost imaging with entangled photons for different types of momentum correlation

MaLin Zhong , Ping Xu*, LiangLiang Lu, and ShiNing Zhu

National Laboratory of Solid State Microstructures and School of Physics, Nanjing University, Nanjing 210093, China

Received February 2, 2016; accepted March 27, 2016; published online May 20, 2016

We present an analytical analysis of the spatial resolution of quantum ghost imaging implemented by entangled photons from a general, spontaneously parametric, down-conversion process. We find that the resolution is affected by both the pump beam waist and the nonlinear crystal length. Hence, we determined a method to improve the resolution for a certain imaging setup. It should be noted that the resolution is not uniquely related to the degree of entanglement of the photon pair since the resolution can be optimized for a certain degree of entanglement. For certain types of Einstein-Podolsky-Rosen (EPR) states——namely the momentum-correlated or momentum-positively correlated states——the resolution exhibits a simpler relationship with the pump beam waist and crystal length. Further, a vivid numerical simulation of ghost imaging is presented for different types of EPR states, which supports our analysis. This work discusses applicable references to the applications of quantum ghost imaging.

resolution of ghost imaging, entangled photons, momentum correlation

PACS number(s): 42.50.-p, 42.65.Lm, 42.70.Mp

Citation: M. L. Zhong, P. Xu, L. L. Lu, and S. N. Zhu, Resolution of ghost imaging with entangled photons for different types of momentum correlation, Sci. China-Phys. Mech. Astron. **59**, 670311 (2016), doi: 10.1007/s11433-016-0056-6

1 Introduction

The entangled photon pairs generated by spontaneous parametric down-conversion (SPDC) exhibit a variety of quantum features that provide critical tests of quantum fundamentals and increase the applications of quantum technologies such as quantum imaging and quantum lithography by utilizing the intrinsic spatial correlations between two photons. Inspired by Klyshko [1,2], the first experimental demonstration of quantum ghost imaging was carried out by Pittman et al. in 1995 [3]. Since then, ghost imaging with biphotons has been extensively investigated [4-7] and was later extended to the regime of thermal light [8-11]. With the in-depth investigations of, e.g., lensless ghost imaging [12-14], three-dimensional ghost imaging [15,16] and the realization of quantum digital spiral imaging [17], increasing attention has been paid to the practical applications of ghost imaging.

One important parameter when considering the practical application of quantum ghost imaging is the spatial resolution. In classical optics, the imaging resolution is determined by the spatial coherence of the light source as well as the imaging setup. For ghost imaging using entangled photons, the resolution of quantum ghost imaging has been discussed in refs. [18-21], which show the relationships between the pump beam waist as well as the wavelength of the entangled photons and the external optical setup by assuming that the two-photon momentum proceeds in an anticorrelated fashion [19]. In ref. [21], even though the influence of the crystal length on the resolution is taken into account, the numerical results do not fit for the state generated by a very long crystal. In this work, we focus on a general two-photon state that contains both correlated and anticorrelated momentum terms and determine the spatial resolution for different types of momentum correlation. We find that the resolution can be

*Corresponding author (email: pingxu520@nju.edu.cn)

improved by altering either the crystal length or pump beam waist. In particular, the resolution can be enhanced monotonically by increasing the pump beam waist or decreasing the crystal length when the two-photon momenta show anti-correlation. Furthermore, the resolution can be enhanced by increasing the crystal length or decreasing the pump beam waist in a momentum-positively correlated (MPC) state. The resolution of quantum ghost imaging is not uniquely related with the degree of spatial entanglement since the resolution can be optimized to its minimum for a certain degree of entanglement. Moreover, we also show the influence of a real experimental setup on the spatial resolution by analytical and numerical calculations.

2 Biphoton amplitude

Let us consider periodically poled lithium niobate (PPLN), which can offer a high-efficiency nonlinear interaction in a quasi-phase-matching way [22,23]. The QPM SPDC can ensure a long collinear interaction between the pump, the signal, and the idler; therefore, it can be adopted for studying a two-photon state, wherein the crystal length can be freely extended. The general two-photon state when the pump beam waist and crystal length are taken into account is given as follows [19, 24-26]:

$$\Psi(\boldsymbol{q}_s,\boldsymbol{q}_i)\propto\exp\left[-\frac{|\boldsymbol{q}_s+\boldsymbol{q}_i|^2\omega_p^2}{4}\right]\mathrm{sinc}\left[\frac{|\boldsymbol{q}_s-\boldsymbol{q}_i|^2L}{4k_p}\right]. \tag{1}$$

Here, we are interested in the spatial correlation between the signal and the idler considering the signal and idler in a single-frequency mode, which can be further justified experimentally through the use of narrow-band interference filters in the detection system.

To obtain a theoretical characterization of ghost imaging, we need to describe the propagation of down-converted photons from the nonlinear crystal through the respective optical elements to the detection planes (see Figure 1). The biphoton amplitude for detectors D_1 (bucket detector) and D_2 (point detector) located at (z_1+u,ρ_1) and (z_2,ρ_2), respectively, takes

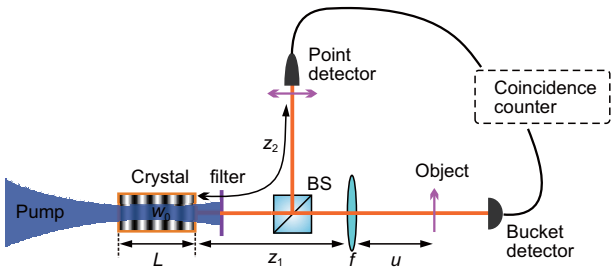

Figure 1 (Color online) Experimental setup for quantum ghost imaging. The SPDC in PPLN crystal produces spatially entangled photon pairs. The photon pair is split into two paths. In the transmitted path, a lens is placed and followed by the object. A bucket detector (D_1) collects all of the photons passing through the object. The distance from the lens to the crystal (object) is denoted by z_1 (u). In the other path, a point detector (D_2) scans while maintaining the distance z_2 to the crystal.

the form

$$A(\boldsymbol{\rho}_1,\boldsymbol{\rho}_2)=<0|E_2^{(+)}(\boldsymbol{\rho}_2,z_2,t_2)E_1^{(+)}(\boldsymbol{\rho}_1,z_1+u,t_1)|\psi>, \tag{2}$$

where $E_2^{(+)}(\boldsymbol{\rho}_2,z_2,t_2)$ and $E_1^{(+)}(\boldsymbol{\rho}_1,z_1+u,t_1)$ are the positive-frequency parts of the quantized field operators at D_1 and D_2, respectively. In the paraxial approximation, we have

$$E_j^{(+)}\propto\int\mathrm{d}\omega_j\int\mathrm{d}\boldsymbol{q}_j\mathrm{e}^{-\mathrm{i}\omega_j t_j}g(\boldsymbol{q}_j,\omega_j;\boldsymbol{\rho}_j,z_j)a(\boldsymbol{q}_j,\omega_j), \tag{3}$$

where $g(\boldsymbol{q}_j,\omega_j;\boldsymbol{\rho}_j,z_j)$ is the optical transfer function that describes the propagation of each mode from the output surface of the source to the j-th detector at the transverse coordinate $\boldsymbol{\rho}_j$ at a distance from the output surface to the detection plane z_j.

Following the procedure in ref. [27], we evaluate the transfer functions $g(\boldsymbol{q}_1,\omega_s;\boldsymbol{\rho}_1,z_1+u)$ and $g(\boldsymbol{q}_2,\omega_i;\boldsymbol{\rho}_2,z_2)$ for the experimental setup in Figure 1

$$g(\boldsymbol{q}_1,\omega_s;\boldsymbol{\rho}_1,z_1+u)=\iint\mathrm{d}\boldsymbol{\rho}_{s1}\mathrm{d}\boldsymbol{\rho}_f h_\omega(\boldsymbol{\rho}_1-\boldsymbol{\rho}_f,u)S(\boldsymbol{\rho}_f)\cdot h_\omega(\boldsymbol{\rho}_f-\boldsymbol{\rho}_{s1},z_1)\exp(\mathrm{i}\boldsymbol{q}_1\boldsymbol{\rho}_{s1}), \tag{4}$$

$$g(\boldsymbol{q}_2,\omega_i;\boldsymbol{\rho}_2,z_2)=\int\mathrm{d}\rho_{s2}h_\omega(\boldsymbol{\rho}_2-\boldsymbol{\rho}_{s2},z_2)\exp(\mathrm{i}\boldsymbol{q}_2\boldsymbol{\rho}_{s2}), \tag{5}$$

where

$$h_\omega(\rho,z)=-\mathrm{i}\omega\exp(\mathrm{i}\omega z/c)\exp(\mathrm{i}\omega\rho^2/2zc)/(2\pi zc), \tag{6}$$

and the transmittance function of the lens is $S(\rho_f)=\exp[-\mathrm{i}\omega\rho_f/(2cf)]t(\rho_f)$. Here, we assume the lens has an infinite aperture, namely $t(\rho_f)=1$. In terms of these optical transfer functions, we can write the biphoton joint amplitude in the position representation as:

$$A(\boldsymbol{\rho}_1,\boldsymbol{\rho}_2)\propto\iint\mathrm{d}\boldsymbol{q}_1\mathrm{d}\boldsymbol{q}_2g(\boldsymbol{q}_s,\omega_1;\boldsymbol{\rho}_1,z_1+u)\times g(\boldsymbol{q}_i,\omega_2;\boldsymbol{\rho}_2,z_2)\langle0|\hat{a}_{q_1}\hat{a}_{q_2}|\psi\rangle. \tag{7}$$

Without loss of generality, we consider only one spatial dimension for simplicity in the following calculation. Thus, with the use of eqs. (3)-(6), the biphoton amplitude becomes

$$A(\rho_1,\rho_2)\propto\iint\mathrm{d}q_1\mathrm{d}q_2\mathrm{e}^{-\frac{(q_s+q_i)^2w_0^2}{4}}\mathrm{sinc}\left[\frac{(q_s-q_i)^2L}{4k_p}\right]\times\iint\mathrm{d}\rho_{s1}\mathrm{d}\rho_{s2}\mathrm{e}^{\frac{\mathrm{i}\omega(\rho_{s1}-\rho_f)^2}{2cz_1}}\mathrm{e}^{\frac{\mathrm{i}\omega(\rho_{s2}-\rho_2)^2}{2cz_2}}\times\int\mathrm{d}\rho_f\mathrm{e}^{\frac{\mathrm{i}\omega(\rho_f-\rho_1)^2}{2cu}}\mathrm{e}^{-\frac{\mathrm{i}\omega\rho_f^2}{2cf}}\mathrm{e}^{\mathrm{i}q_1\rho_{s1}}\mathrm{e}^{\mathrm{i}q_2\rho_{s2}}. \tag{8}$$

In the collinear phase-matching regime, the phase-matching term can be simplified by using a Gaussian exponential function that accurately retains the main features of the entanglement of the wave function. Therefore, we take $\mathrm{sinc}[bx^2]\simeq\exp[-bx^2/\xi_0]$ with $\xi_0=1.38$ so that both functions coincide

at the $1/e^2$ intensity. Completing the integrations with respect to the position coordinate in eq. (8) leads to

$$A(\rho_1,\rho_2)\propto\exp\Big[-\frac{(\rho_2-\alpha\frac{z_1+z_2}{u}\rho_1)^2+\frac{4\xi_0\xi}{(\xi_0+\xi)^2}(\frac{z_1+z_2}{u}\rho_1)^2}{4\Delta^2}\Big], \tag{9}$$

where

$$\Delta^2=\frac{\frac{\beta^2\xi_0}{w_0^2}+\frac{L}{k_p}}{\xi_0+\xi}, \tag{10}$$

with $\beta=\lambda_s z_2/2\pi$. $\xi=L/(\omega_0^2 k_p)$ and is the focal parameter, and

$$\alpha=\frac{\xi-\xi_0}{\xi_0+\xi}. \tag{11}$$

In addition, $\frac{1}{z_1+z_2}+\frac{1}{u}=\frac{1}{f}$ is satisfied.

3 Resolution of ghost imaging and discussion

In parallel, the properties of the ghost imaging of photon pairs can be studied by counting the coincidences between two spatially separated single-photon detectors. The rate of the coincidence counts is related to the second-order correlation function

$$G^{(2)}(\rho_1,z_1+u;\rho_2,z_2)=\langle\psi|a^\dagger(\rho_2)a^\dagger(\rho_1)a(\rho_1)a(\rho_2)|\psi\rangle \propto|A(\rho_1;\rho_2)|^2, \tag{12}$$

which indicates a point-to-spot correspondence between the object and the ghost image planes. It is noted that the remaining term of ρ_1^2 in eq. (9) will become different constant backgrounds for different positions on the detection planes. Moreover, the uncertainty in the position correlation Δ and $\alpha\frac{z_1+z_2}{u}$ are the resolution and magnification of the ghost image, respectively [19].

The magnification consists of two parts, α and $\frac{z_1+z_2}{u}$, which are defined as the intrinsic and extrinsic magnifications. The extrinsic magnification $\frac{z_1+z_2}{u}$ depends on the setup of the imaging system, which is defined by the ratio of the equivalent imaging distance to the object distance. In contrast, the intrinsic magnification α uniquely depends on the focal parameter ξ, which also uniquely determines the type of the two-photon momentum correlation [24]. In other words, the magnification would be different for different two-photon momentum (or position) correlations, even though the object and image distances are fixed. For the ideal MPC (anticorrelated) state, namely $\xi\gg\xi_0$ ($\xi\ll\xi_0$), the magnification is $\frac{z_1+z_2}{u}$ ($-\frac{z_1+z_2}{u}$), corresponding to noninverted (inverted) ghost imaging. However, ghost imaging cannot be realized for the decorrelated state, i.e., $\xi=\xi_0$, which leads to $\alpha=0$. The general relation for α depending on ξ is shown in Figure 2(a).

Moreover, we consider the degree of entanglement. In order to quantify the amount of entanglement, we resort to the Schmidt decomposition. This given information about the degree of entanglement of the state via the Schmidt number K, which is defined as the average number of nonzero coefficients in the Schmidt decomposition. For the double-Gaussian form, one can find the Schmidt decomposition in an analytical form [28]. The curve of the Schmidt number is shown in Figure 2(a), which, in comparison with the absolute value of α, shows a unique dependence on ξ and follows the same trend as that of K. Hence, one can identify the entanglement and correlation of two photons by measuring the intrinsic magnification in ghost imaging experiments instead of measuring the correlation in the near and far fields of the photons [29].

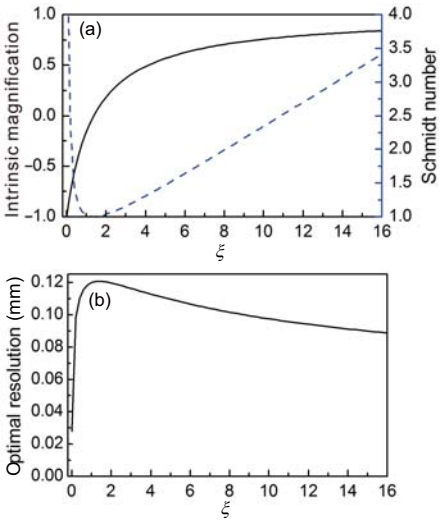

Figure 2 (Color online) (a) The relation between the intrinsic magnification α and the focal parameter ξ and the curve of the Schmidt number, which quantifies the degree of entanglement; (b) the relation between the optimal resolution and ξ, which shows the corresponding relation with the degree of entanglement.

As mentioned above, Δ is defined as the resolution of the ghost image. In its expression, the resolution is dependent on ξ, which determines the degree of entanglement, and on the specific experimental setup, which includes the parameters z_2, w_0, and L. In other words, the imaging resolution will not necessarily improve with an increase in the degree of entanglement. However, the optimal resolution can be given by $\Delta_m=\sqrt{2\beta\sqrt{\xi_0\xi}/(\xi_0+\xi)}$ for a certain value of ξ by choosing the proper experimental parameters that satisfy $\beta^2\frac{\xi_0}{w_0^2}=\frac{L}{k_p}=\beta\sqrt{\xi_0\xi}$. Figure 2(b) shows the relation between the optimal resolution and ξ.

In comparison with the curve of Schmidt number in Figure 2(a), the optimal resolution has a corresponding relation with the degree of entanglement. Namely, a worse imaging resolution is obtained for a lower degree of entanglement, whereas a better optimal resolution is obtained for a higher degree of entanglement. It is noted that the conditions for obtaining the optimal resolution can be easily achieved for the EPR state, but it is difficult to satisfy the conditions for the CEPR state because a long crystal length $L=k_p\beta\sqrt{\xi_0\xi}$ is required.

Generally, the experimental setup does not satisfy the conditions for the optimal resolution. To analyze the effect of the experimental setup on the resolution in a general situation, one can rewrite eq. (10) as:

$$\Delta^2 = w_0^2 + \frac{\beta^2 - w_0^4}{\frac{L}{\xi_0 k_p} + w_0^2}, \tag{13}$$

or

$$\Delta^2 = \frac{L}{\xi_0 k_p} + \frac{(\beta k_p \xi_0)^2 - L^2}{(w_0 k_p \xi_0)^2 + L k_p \xi_0}. \tag{14}$$

As we are mainly concerned about L and w_0, we assume that z_2, i.e., β, is fixed. Thus, the critical value of the pump beam waist $w_{0c} = \sqrt{\beta}$ is given from eq. (13). When $w_0 > w_{0c}$, the resolution for ghost imaging is a monotonically increasing function of L, which means that the resolution can be optimized by decreasing the crystal length. Correspondingly, the resolution can be optimized by increasing the crystal length for $w_0 < w_{0c}$. Similarly, a critical crystal length $L_c = \beta k_p \xi_0$ is given from eq. (14). When $L > L_c$, the resolution is an increasing function of w_0. One can optimize the resolution by decreasing the pump beam waist. In contrast, a larger pump beam waist is needed for $L < L_c$ to obtain a better resolution. In Figure 3, we show a simulation of the imaging resolution for three different values of w_0 as a function of L/L_c. In the simulation, we assumed that $\lambda_s = 914$ nm and $z_2 = 50$ mm such that we have $w_{0c} = 85.3$ μm and $L_c = 303$ mm.

Now, we turn to two specific cases. For the momentum-correlated EPR state, it is usually generated when $w_0 > w_{0c}$; then, if $L \ll L_c$, i.e., $\xi \ll 1$, the spatial resolution can be enhanced by simply increasing the pump beam waist or decreasing the crystal length. Moreover, the limit of the resolution, $\Delta = \sqrt{\frac{L}{\xi_0 k_p}}$, can be obtained from eq. (14) by taking the limit as the pump beam waist tends to infinity. In other words, the effect of L cannot be neglected for a large w_0. In contrast, the MPC-EPR state usually generated when $w_0 < w_{0c}$; thus, when $L \gg L_c$, i.e., $\xi \gg 1$ in this case, the resolution can be enhanced by simply increasing the crystal length or decreasing the pump beam waist.

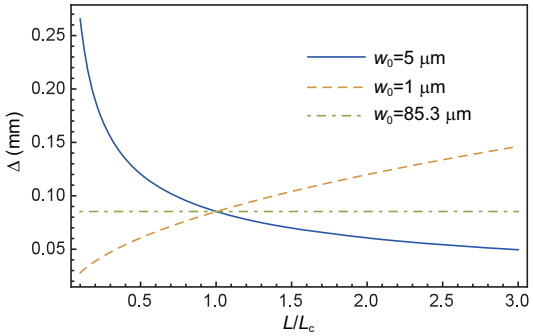

Figure 3 (Color online) The imaging resolution for three different pump beam waists w_0 as a function of L/L_c. In the simulation, $\lambda_s = 914$ nm and $z_2 = 50$ mm.

In order to show the influence of the focal parameter on ghost imaging more vividly, we simulate ghost imaging by calculating the rate of coincidence counts between detectors D_1 and D_2. Here, a letter "F" is placed on the object plane as an object. Its transmitting function is shown in Figure 4(a). In the simulation, $\lambda_s = 914$ nm, $z_2 = 50$ mm, and the extrinsic magnification $(z_1 + z_2)/u = 1/2$. The quantum ghost images for different focal parameters, i.e., different states, are shown in Figures 4(b)-(f). Specifically, L (ω_0) is 1 mm (1 mm) and 1 mm (0.05 mm) for Figures 4(b) and (c), respectively, corresponding to the EPR states. As shown, the image is inverted, and the imaging quality becomes worse when decreasing the pump beam waist ω_0 with L fixed. In Figure 4(d), $L = 10$ mm, $\omega_0 = 0.015$ mm, and the focal parameter $\xi = 1.47$ is close to ξ_0. The degree of entanglement of the state generated for these parameters is quite small, and its intrinsic magnification is very close to zero. Therefore, ghost imaging cannot be realized. In Figures 4(e) and (f), L (ω_0) is 100 mm (0.005 mm) and 500 mm (0.005 mm), respectively. As predicted in ref. [24], the image is noninverted (upright). However, it requires a crystal length as long as 500 mm to achieve the relatively clear imaging shown in Figure 4(f), which is hardly realized in an experiment and promotes future study.

In our theoretical analysis, we find that α has a corresponding relation with the entanglement and correlation of the two-photon pairs. The demarcation point for the EPR and CEPR states is $\alpha = 0$, i.e., $\xi = \xi_0 = 1.38$, whereas the curve of entanglement entropy in ref. [24] gives a demarcation point at $\xi = 1.32$. This acceptable difference is due to the Gaussian exponential approximation of the sinc function in the phase-matching term. Conversely, such an approximation turns out to be reasonable.

Additionally, another approximation in which the lens has an infinite aperture is made in the analysis. Although there actually exists an effect on the resolution caused by the diffraction limit due to the finite size of the imaging lens, such an effect can be negligible in our analysis. In refs. [18,19], the diffraction limit is taken into account because the radius

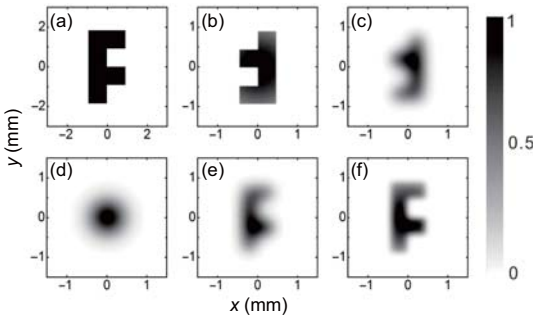

Figure 4 Simulation results for ghost imaging. (a) A letter "F" as an object on the object plane; (b)-(f) the rate of coincidence counts between detectors D_1 and D_2 by scanning D_2 two-dimensionally. In the simulation, $\lambda_s = 914$ nm, $z_2 = 50$ mm, and $(z_1 + z_2)/u = 1/2$. L (ω_0) is 1 mm (1 mm), 1 mm (0.05 mm), 10 mm (0.015 mm), 100 mm (0.005 mm), and 500 mm (0.005 mm) for (b)-(f) respectively.

of the Airy disk may be larger than the uncertainty in the position when the phase-matching function is neglected. However, our approximation is reasonable when the phase-matching function is involved. For a circular aperture, the Airy disk has a radius $\delta = 0.61\frac{\lambda_s}{X_{NA}}$, where $X_{NA} = R_{\text{lens}}/u$, and R_{lens} is the radius of the aperture. We assume that $R_{\text{lens}} = 12.5$ mm and $u = 100$ mm, which gives $\delta = 4.5$ μm——much smaller than $\Delta = 16$ μm for a typical EPR state setup that $L = 2$ mm, and $\omega_0 = 1$ mm.

4 Conclusion

In conclusion, we have studied the resolution of ghost imaging implemented by photon pairs generated from an SPDC inside a nonlinear crystal. The analytical expression of the two-photon amplitude at the detection planes has been derived from the viewpoint of the propagation of biphotons through various optical elements. An analytical calculation gives the magnification and resolution of ghost imaging. The analytical and numerical calculations both show that the influence of the crystal length on the imaging resolution cannot be neglected for a large pump beam waist. Moreover, the resolution is not uniquely dependent on the focal parameter, i.e., the degree of entanglement, but on the specific experimental setup. In particular, the resolution for the ideal EPR state can be optimized by increasing the pump beam waist or decreasing the crystal length, whereas it can be enhanced by increasing the crystal length or decreasing the pump beam waist for the MPC-EPR state. We believe that these results can lead to an enhanced quantitative and qualitative understanding of ghost imaging under realistic experimental conditions and may bring about optimized experimental implementations.

This work was supported by the National Natural Science Foundation of China (Grant Nos. 11174121, 11321063, 91121001, and 91321312), the National Program on Key Basic Research Project (Grant No. 2012CB921802). P. Xu acknowledges the Program for New Century Excellent Talents in University (NCET), Foundation for the Author of National Excellent Doctoral Dissertation of China (FANEDD).

1 D. N. Klyshko, Sov. Phys. Usp. **31**, 74 (1988).
2 D. N. Klyshko, Phys. Lett. A **132**, 299, (1988).
3 T. B. Pittman, Y. H. Shih, D. V. Strekalov, and A. V. Sergienko, Phys. Rev. A **52**, R3429 (1995).
4 T. B. Pittman, D. V. Strekalov, D. N. Klyshko, M. H. Rubin, A. V. Sergienko, and Y. H. Shih, Phys. Rev. A **53**, 2804 (1996).
5 M. D'Angelo, M. V. Chekhova, and Y. H. Shih, Phys. Rev. Lett. **87**, 013602 (2001).
6 M. D'Angelo, Y. H. Kim, S. P. Kulik, and Y. Shih, Phys. Rev. Lett. **92**, 233601 (2004).
7 G. Scarcelli, A. Valencia, and Y. Shih, Europhys. Lett. **68**, 618 (2004).
8 A. Valencia, G. Scarcelli, M. D'Angelo, and Y. H. Shih, Phys. Rev. Lett. **94**, 063601 (2005).
9 R. S. Bennink, S. J. Bentley, and R. W. Boyd, Phys. Rev. Lett. **89**, 113601 (2002).
10 A. Gatti, E. Brambilla, M. Bache, and L. A. Lugiato, Phys. Rev. Lett. **93**, 093602 (2004).
11 R. Meyers, K. S. Deacon, and Y. H. Shih, Phys. Rev. A **77**, 041801(R) (2008).
12 G. Scarcelli, V. Berardi, and Y. H. Shih, Appl. Phys. Lett. **88**, 061106 (2006).
13 L. Basano, and P. Ottonello, Appl. Phys. Lett. **89**, 091109 (2006).
14 Z. Yang, L. J. Zhao, X. L. Zhao, W. Qin, and J. L. Li, Chin. Phys. B **25**, 024202 (2016).
15 Y. Hong, E. R. Li, W. L. Gong, and S. S. Han, Opt. Express **23**, 14541 (2015).
16 X. Yang, Y. Zhang, L. Xu, C. H. Yang, Q. Wang, Y. H. Liu, and Y. Zhao, Chin. Phys. B **24**, 124202 (2015).
17 L. Chen, J. Lei, and J. Romero, Light-Sci. Appl. **3**, e153 (2014).
18 M. H. Rubin, and Y. H. Shih, Phys. Rev. A **78**, 033836 (2008).
19 M. D'Angelo, A. Valencia, M. H. Rubin, and Y. H. Shih, Phys. Rev. A **72**, 013810 (2005).
20 J. M. Wen, S. W. Du, and M. Xiao, Phys. Lett. A **374**, 3908 (2010).
21 A. F. Abouraddy, B. E. A. Saleh, A. V. Sergienko, and M. C. Teich, J. Opt. Soc. Am. B **19**, 1174 (2002).
22 J. A. Armstrong, N. Bloembergen, J. Ducuing, and P. S. Pershan, Phys. Rev. **127**, 1918 (1962).
23 P. A. Franken, and J. F. Ward, Rev. Mod. Phys. **35**, 23 (1963).
24 S. J. Yun, P. Xu, J. S. Zhao, Y. X. Gong, Y. F. Bai, J. Shi, and S. N. Zhu, Phys. Rev. A **86**, 023852 (2012).
25 J. P. Torres, A. Alexandrescu, S. Carrasco, and L. Torner, Opt. Lett. **29**, 376 (2004).
26 M. L. Zhong, P. Xu, L. L. Lu, and S. N. Zhu, J. Opt. Soc. Am. B **32**, 2081 (2015).
27 M. H. Rubin, Phys. Rev. A **54**, 5349 (1996).
28 S. S. Straupe, D. P. Ivanov, A. A. Kalinkin, I. B. Bobrov, and S. P. Kulik, Phys. Rev. A **83**, 060302(R) (2011).
29 J. C. Howell, R. S. Bennink, S. J. Bentley, and R. W. Boyd, Phys. Rev. Lett. **92**, 210403 (2004).